Radionuclide Removal from Aqueous Solutions by Oxidized Carbon Fabrics

Ioannis Ioannidis *, Ioannis Pashalidis, Batuhan Mulla, Gkerman Kotanidis, Kyriacos Ioannou, Georgios Constantinides, Nikolaos Kostoglou, Claus Rebholz *

Posted Date: 13 November 2023

doi: 10.20944/preprints202311.0743.v1

Keywords: U-232; Am-241; radioactivity; radionuclide removal; oxidized carbon fabrics; water treatment

Article

Radionuclide Removal from Aqueous Solutions by Oxidized Carbon Fabrics

Ioannis Ioannidis [1,*], Ioannis Pashalidis [1], Batuhan Mulla [2], Gkerman Kotanidis [2], Kyriacos Ioannou [2], Georgios Constantinides [3], Nikolaos Kostoglou [4] and Claus Rebholz [2,*]

[1] Department of Chemistry, University of Cyprus, P.O. Box 20537, 1678 Nicosia, Cyprus
[2] Department of Mechanical and Manufacturing Engineering, University of Cyprus, 1 Panepistimiou Avenue, 2109 Nicosia, Cyprus
[3] Department of Mechanical Engineering and Materials Science and Engineering, Cyprus University of Technology, 3036 Lemesos, Cyprus
[4] Department of Materials Science, Montanuniversität Leoben, Franz Josef-Strasse 18, 8700 Leoben, Austria
* Correspondence: iioann03@ucy.ac.cy,(II); rebholz.claus@ucy.ac.cy, (CR)

Abstract: The adsorption of actinide ions (Am(III) and U(VI)) from aqueous solutions by pristine and oxidized carbon fabrics has been investigated by means of batch experiments at different pH values (4, 7 and 9) and temperatures (25, 35 and 45 °C) under ambient atmospheric conditions. The experimental results indicate that both pH and fabric texture affect the adsorption rate and the relative removal efficiency, which results at 70% and 100% for Am(III) and U(VI), respectively. The K_d (L/kg) values for U(VI) have been generally found to be higher ($2 < \log_{10}(K_d) < 3$) than the corresponding values for the Am(III) adsorption ($1.5 < \log_{10}(K_d) < 2$). The data obtained from the experiments regarding the temperature effect imply that the relative adsorption for both actinides increases with temperature and that the adsorption is an endothermic and entropy-driven reaction. Application of the fabrics to remove the two actinides from contaminated seawater samples shows that both the relative removal efficiency and the K_d values decrease significantly due to the presence of competitive cations (e.g., Ca^{2+} and Fe^{3+}) and complexing anions (CO_3^{2-}) in the respective waters. Nevertheless, the removal efficiency is still remarkable (50% and 90% for Am(III) and U(VI), respectively), demonstrating that these materials could be attractive candidates for the treatment of radionuclide/actinide contaminated waters.

Keywords: U-232; Am-241; radioactivity; radionuclide removal; oxidized carbon fabrics; water treatment

1. Introduction

The removal of radionuclides from contaminated waters (e.g., wastewater) prior to their release in the ocean or other environmental receivers is obligatory to protect the environment [1]. The present study deals with the removal of two actinide elements, uranium and americium, by means of their isotopes U-232 and Am-241, respectively. Uranium is a naturally occurring element and is found in the form of different isotopes, which are all radioactive with half-life varying between 1.59×10^5 and 4.47×10^9 years [2]. The most abundant uranium isotopes in nature are U-238 (99.3%) and U-235 (0.7%) [3]. The latter is a fissile radionuclide and is widely used as fuel in nuclear power reactors and nuclear weapons [4,5]. On the other hand, americium is a man-made element which is formed when plutonium absorbs neutrons during nuclear power production or nuclear power tests [6,7]. The most common isotopes of americium are Am-241 and Am-243 with half-life of 432.2 and 7350 years, respectively. Am-241 is widely used in household smoke detectors and lightning rods. Furthermore, Am-241 has been also used as alpha- and gamma-particle source for medical and industrial applications [6,8]. It is obvious that, due to improper disposal of smoke detectors or even lightning rods, americium may enter landfills and disperse into the environment.

Uranium under ambient conditions exists basically in its hexavalent form as uranyl cation (UO_2^{2+}) and in environmental waters can undergo hydrolysis [6,9], carbonate complexation [10,11], interact with inorganic and organic colloids and mineral/rock surfaces [12, 13]. In seawater the U(VI)-tricarbonato complex ($UO_2(CO_3)_3^{4-}$) is the prevailing U(VI) species and stabilizes uranium in the

 doi:10.20944/preprints202311.0743.v1

aqueous phase. Under anoxic/reducing conditions reduction of U(VI) to U(IV) is also possible [14,15]. The trivalent oxidation state is the predominant oxidation state of americium in aqueous solutions and its chemical behaviour is similar to the chemical behaviour of trivalent lanthanides (e.g., Eu(III)) [16,17].

There are many methods (e.g., reverse osmosis, precipitation) to remove pollutants, including radionuclides, from waste and process waters [18-21]. However, the low-cost and ease of operation as well as the wide spectrum of adsorbent materials available make adsorption-based technologies very attractive regarding the removal of pollutants [22-24]. In this respect, lightweight nanoporous carbon-based materials, including activated carbons, have been suggested as a promising category of adsorbents for the removal of pollutants from water sources due to their large surface areas and pore volumes, tunable and hierarchical pore structures and high adsorption capacities [25]. However, most of the commercial and lab-synthesized carbons are usually produced as fine and volatile powders, which could lead to potential issues concerning health, handling and practicality [26-28]. Instead, carbons produced in a more compacted form, including monoliths and cloths, are more likely to be used as functional components in commercial water purification systems and large-scale water treatment applications. For example, activated carbon cloth materials have attracted increasing interest over the last decade not only for wastewater treatment applications [29-32] but also for capacitive deionization [33], gas storage [34-36] and gas separation [35-37].

Hence, in this study, activated carbon fiber fabrics have been used as flexible, robust and self-standing/binder-free adsorption-based filters for the removal of radionuclides (e.g. U-232 and Am-241) from laboratory solutions and seawater samples. The selected carbon fabrics demonstrate different macroscopic fibrous morphologies (i.e., woven, non-woven, felt) and pore structure characteristics (i.e., surface areas, pore volumes, pore sizes), as determined by scanning electron microscopy (SEM) and N_2 adsorption tests. To move a step further, the same carbon fabrics have been also controllably oxidized by chemical means with the aim to introduce surface oxygen-based functionalities, which could act beneficially for the removal of pollutants from water, as shown in a previous study [38]. Recently, Zulfiqar et al. (2021) reported a surface functionalized carbon cloth that showed efficient separation of various types of oil-water mixtures under neutral, basic and acidic conditions [39]. Fourier-transform infrared (FTIR) and X-ray photoelectron spectroscopy (XPS) were also employed to investigate the differences in the surface chemistry and elemental composition between the pristine and oxidized carbon fabrics.

2. Materials and Methods

2.1. Materials

The tracer solutions employed in this study were Am-241 (supplied by North America Scientific Inc. in Los Angeles, CA, USA) and U-232 (provided by the National Physical Laboratory in Teddington, UK), both possessing activity concentrations of 12.05 and 4.923 kBq/g, respectively. These tracer standard solutions were utilized to create reference and test solutions, initially containing 25 Bq/L for each radionuclide, which equates to approximately 0.1 pmol/L for both Am-241 and U-232.

2.2. Methods

2.2.1. Carbon fabric oxidation and characterization

The three activated carbon fabrics used in this study (denoted hereafter as woven, non-woven and felt) were provided by Evertech Envisafe Ecology (Taiwan) and were controllably oxidized in the lab with concentrated HNO_3 (8 M). A detailed description of the oxidation procedure of the fabrics is provided in a previous study [40]. It has been shown earlier that surface oxidation and formation of oxygen containing moieties such as carboxylic groups, promote the interaction between metal ions and the biochar surface [38]. The three oxidized carbon fabrics are denoted hereafter as ox-woven, ox-non-woven and ox-felt, respectively.

 doi:10.20944/preprints202311.0743.v1

SEM images were collected with an FEI Quanta 200 microscope using a 20 kV acceleration voltage and a working distance of approximately 10 mm. Prior to SEM analysis, a thin (a few nm) film of Au was deposited using sputter coating to improve surface conductivity and avoid potential charging effects during imaging. Images were collected at magnifications in the range of x100 to x20,000 in order to study their microstructural characteristics.

Surface area and pore structure analysis was performed by means of N_2 adsorption/desorption at -196 ^{o}C using a manometric gas sorption analyzer (Anton-Paar QuantaTec Autosorb iQ$_3$). He and N_2 gases of ultra-high purity (99.999%) were employed for void volume calculations and gas sorption analysis, respectively. Prior to the tests, samples of ~40 mg were degassed under high vacuum (10^{-6} mbar) at 250 ^{o}C for 24 h to remove physisorbed water from their surface and make the pore structure more accessible. The specific surface area (SSA) was calculated using the multi-point Brunauer-Emmet-Teller (BET method), following the BET consistency criteria of the International Standard Organization (ISO 9277:201). The specific pore volume (SPV) was calculated using the single-point Gurvich rule at relative pressures close to unity. The average pore width (W) was estimated using the ratio 2·SPV/SSA, upon assuming an infinitely extended slit-like pore system. XPS studies were carried out by a Thermo Scientific Theta Probe spectrometer equipped with a monochromated Al Kα radiation source (hv = 1486.6 eV) using an X-ray spot of ~400 mm in radius. Survey spectra were acquired using a pass energy of 300 eV, while a high-resolution core level spectrum for the C1s component was acquired with a pass energy of 50 eV. All spectra were charge referenced against the C1s peak at 284.5 eV (sp^2 hybridized carbon) to correct for charging effects during acquisition. Quantitative chemical compositions were determined from the high-resolution core level spectra, using instrument modified Wagner sensitivity factors, following the removal of a non-linear Shirley background. FTIR spectra were recorded by using a FTIR spectrometer 8900, Shimadzu.

2.2.2. Adsorption experiments

The sorption experiments were performed in 20 mL polyethylene (PE) vials under ambient conditions at 23 ± 2 ^{o}C. The experiments were performed in artificial solutions using deionized water at different pH values (4, 7 and 9). The analysis of U-232 and Am-241 was carried out using an alpha-spectrometer (Canberra) after electrodeposition of uranium on stainless steel discs, as described elsewhere [41].

All sorption experiments were carried out by contacting 0.05 g of oxidized fabrics in artificial radionuclide solution (U-232 and Am-241) of a total volume of 10 ml. The contents of the flasks were stirred in a linear stirrer (SK-R1807, DLAB) at a constant stirring rate (45 min^{-1}). At specified time intervals, a small amount (50 μL) was withdrawn from the solution and electrodeposited to determine the adsorbed activity of the radionuclides. The radionuclides concentration in the solution was calculated with an alpha spectrometer. Spectrometer calibration was performed using a standard reference solution and a calibration source (1.02 Bq/mL U-232 standard reference solution and 6.6 Bq (total) U-238/234, Pu-239, Am-241 mixed standard on planchet by Eckert & Ziegler).

The trace amounts of uranium and americium isotopes used are extremely low. Relative to the initial concentration of radionuclides, surface binding sites (B) are expected to be in large excess. Therefore, to express the mass action of radiometal adsorption, the distribution coefficient K_d can be used:

$K_d = C_{ads}/C_{aq}$ (L/Kg) (1)

C_{ads} (Bq/g) = the amount of radionuclide adsorbed by the fabrics

C_{aq} (Bq/L) = the radionuclides concentration in solution at equilibrium

The amount of uranium and americium adsorbed by the fabrics is calculated from the total amount of radionuclides adsorbed minus the relative amount of radionucleotides adsorbed by the plastic walls of the flask. The amount of radionucleotide adsorbed from the walls of the flask is not negligible and must be taken into account when adsorption experiments are performed using super-trace levels. The percent adsorbed is calculated as the percent adsorbed amount of radioisotope in the test solution relative to the amount of radioisotope in the reference solution. Experiments were

 doi:10.20944/preprints202311.0743.v1

performed in duplicate and mean values have been used for data evaluation and graphical presentations.

3. Results and discussion

3.1. Carbon fabric characterization

Both categories of pristine and oxidized carbon fabrics were characterized for their pore structure, morphology, surface chemistry and elemental composition using N_2 adsorption, SEM, FTIR and XPS, respectively. Table 1 shows the pore structure properties, including specific surface area, specific pore volume and average pore width, as derived by the analysis of N_2 adsorption data using the BET method, the Gurvich rule and a combination of both, respectively.

Table 1. Pore structure properties for the pristine and oxidized carbon fabrics derived by N_2 adsorption data recorded at 77 K.

Material	S_{BET} [m²/g]	$V_{Gurvich}$ [nm]	W [nm]
Woven	1119	0.47	0.84
Ox-woven	560	0.29	1.03
Non-woven	1845	0.86	0.93
Ox-non-woven	532	0.32	1.20
Felt	1080	0.49	0.90
Ox-felt	475	0.25	1.05

*S_{BET}: Brunauer-Emmet-Teller (BET) surface area, $V_{Gurvich}$: total pore volume at P/P_0 ~0.95 for pores smaller than 50 nm in width calculated by the single-point Gurvich rule, **W**: average pore width calculated by the ratio of $2\cdot(V_{Gurvich})/(S_{BET})$ assuming a slit pore model.

For the pristine samples, non-woven exhibits the highest surface area and pore volume among all samples, followed by very comparable values between the woven and felt samples. The average pore widths for all pristine samples seem to range between 0.8 and 1 nm, indicating microporosity (i.e., pore sizes below 2 nm) according to the IUPAC nanopore classification [42]. Upon oxidation all samples showed a significant decrease of their surface areas and pore volumes along with a slight increase of their average pore widths. More specifically, the surface area and pore volume values dropped by 71%, 50% and 56% and by 63%, 38% and 49% for ox-non-woven, ox-woven and ox-felt, respectively, compared to their non-oxidized counterparts. The average pore sizes of the oxidized samples shifted to higher values (i.e., between 1-1.2 nm), remaining however in the microporosity range.

SEM images for the oxidized carbon fabrics at three different magnifications, covering three orders of magnitude in length (i.e., from mm to μm), are illustrated in **Figure 1.** The macroscopic morphological features are highlighted in **Figures 1(a), (d)** and **(g).** The ox-woven sample is knitted from yarns that form a continuous fabric (**Figure 1(a)**), with each yarn spanning several hundreds of microns in width (i.e., up to ~400 μm) and consisting of tens of individual carbon fibers (**Figure 1(b)**). Instead, the ox-non-woven (**Figures 1(d)-(e)**) and ox-felt (**Figures 1(g)-(h)**) samples seem to exhibit a more random "spaghetti"-like distribution of carbon fibers. The SEM images at the highest magnification (**Figures 1(c), (f)** and **(i)**) reveal that, for all three cases, the carbon fibers are internally dense (not hollow), show a corrugated circumference and have diameters in the range of 10-15 μm. It should be noted that all samples maintain the fibrous morphology of their non-oxidized counterparts.

Preprints (www.preprints.org) | NOT PEER-REVIEWED | Posted: 13 November 2023 doi:10.20944/preprints202311.0743.v1

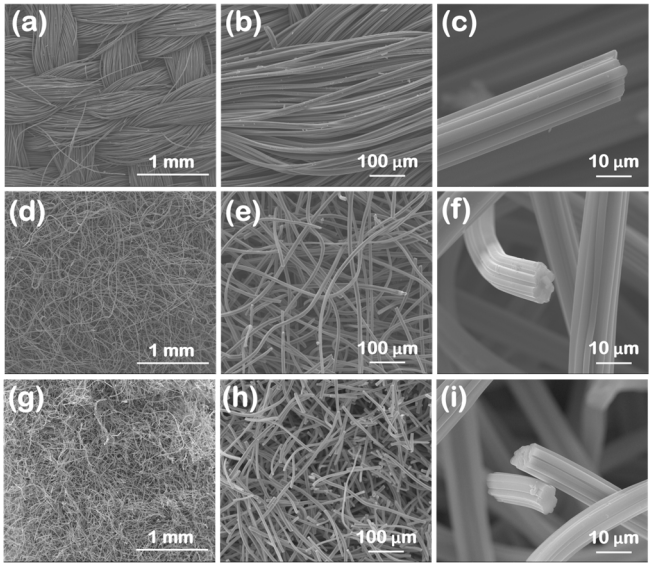

Figure 1. SEM images at different magnifications of the three oxidized carbon fabrics after oxidation with boiling 8 M HNO_3. (woven (**a**)-(**c**), non-woven (**d**)-(**f**) and felt (**g**)-(**i**)).

Figure 2 shows the FT-IR spectra of the three fabric samples (woven, non-woven and felt) prior and after oxidation. Comparison of the spectra prior and after oxidation clearly indicates successful modification of the fabric surface associated with the introduction of oxygen containing moieties. Specifically, the peaks at 1695 cm^{-1}, 1520 cm^{-1} and 1200 cm^{-1}, which correspond to –COO– and –C–O–C– vibrations, respectively, indicate the presence of carbonyl and carboxylic moieties on the fabric surface upon chemical oxidation [38]. It is notable that in the case of the woven fabric the spectrum after oxidation differs significantly from the non-woven and felt and the carbonyl peak at 1810 cm^{-1} is indicating rather carboxylic anhydrites. On the other hand, the peak at 3395 cm^{-1} could be ascribed to hydroxyl groups and water adsorbed on the material's surface.

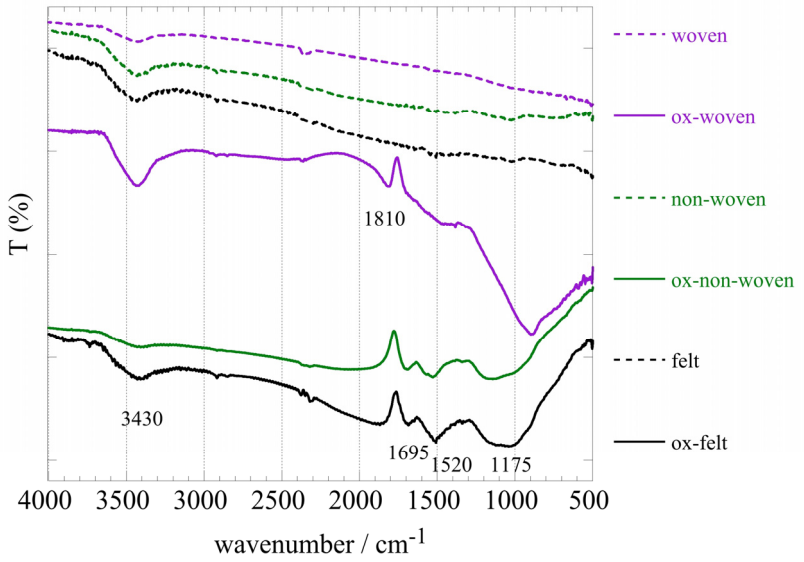

Figure 2. FTIR (KBr) spectra of the three oxidized carbon fabrics (woven, non-woven and felt) prior and after oxidation with boiling 8 M HNO_3.

Table 2 reveals the elemental compositions of all fabric samples before and after oxidation, as derived by XPS analysis. The pristine/non-oxidized samples demonstrate a high carbon purity (i.e., between ~84-91 at.%), followed by oxygen (i.e., between ~8-12 at.%) and much lower concentrations

Preprints (www.preprints.org) | NOT PEER-REVIEWED | Posted: 13 November 2023 doi:10.20944/preprints202311.0743.v1

of nitrogen (i.e., between 0.5-3.5 at.%). Traces of phosphorus (P), silicon (Si) and sodium (Na) were also detected. The oxidized samples, however, showed a drop of their carbon content (i.e., between ~72-77 at.%) along with a significant increase of their oxygen content (i.e., between 21-24 at.%) and a small increase of their nitrogen content (i.e., between 2-4 at.%). The aforementioned P, Si and Na traces were not detected anymore after the oxidation procedure. The XPS findings agree well with the observations of the FTIR spectra, thus supporting the introduction of oxygen-containing moieties on the fibers.

Table 2. Elemental compositions of pristine and oxidized carbon fabrics based on XPS data.

Material	Element (at.%)					
	C	N	Na	O	P	Si
Woven	83.5	3.6	0.1	11.7	0.9	0.2
Ox-woven	72.3	3.8	--	23.8	0.2	--
Non-woven	90.5	0.5	0.5	7.5	0.5	0.6
Ox-non-woven	75.6	1.6	0.1	22.6	--	--
Felt	89.6	1.3	0.3	8	0.5	0.2
Ox-felt	76.8	2.1	--	21.1	--	--

3.2. Radionuclide Adsorption

Figure 3 summarizes the relative removal efficiency determined for the adsorption of the two radionuclides (U-232 and Am-241) by the three oxidized carbon fabrics under acidic (pH 4), neutral (pH 7) and alkaline (pH 9) conditions. According to the collected data (**Figure 3**), uranium is more effectively adsorbed (> 80%) by the fabrics than americium (> 70%). Particularly for uranium, the highest removal efficiency is observed at neutral pH, which is attributed to the partial protonation of the carboxylic groups in the acidic pH range and the stabilization of U(VI), due to the formation of $UO_2(CO_3)_3^{4-}$, in the alkaline pH region. Regarding americium, the three oxidized carbon fabrics present different removal efficiencies at the different pH regions. The ox-non-woven fabric shows almost similar removal efficiency independent of pH, while the removal efficiency of the ox-woven and the ox-felt adsorbents are significantly affected, particularly at pH 9. These possible reactions are schematically depicted in **Figure 4**.

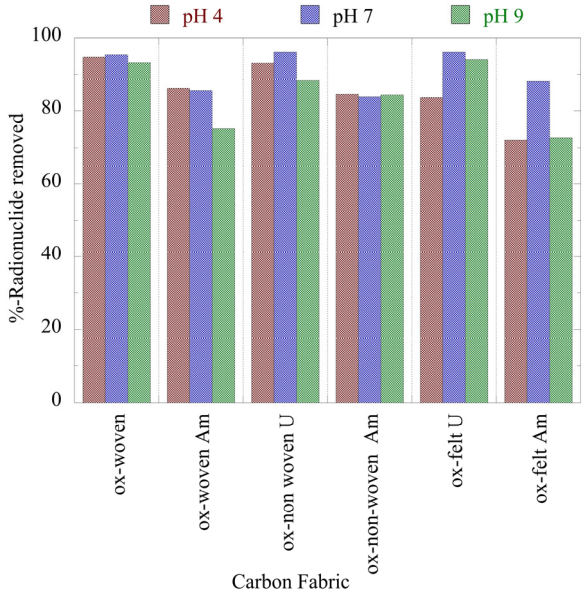

Preprints (www.preprints.org) | NOT PEER-REVIEWED | Posted: 13 November 2023 doi:10.20944/preprints202311.0743.v1

Figure 3. Relative removal of radionuclides (U-232 and Am-241) by the three oxidized carbon fabrics from aqueous solution in the acidic (pH 4), neutral (pH 7) and alkaline (pH 9) region. Experimental conditions: 0.5 Bq/mL tracers of U-232 and Am-241 in 10 mL total volume and ambient conditions.

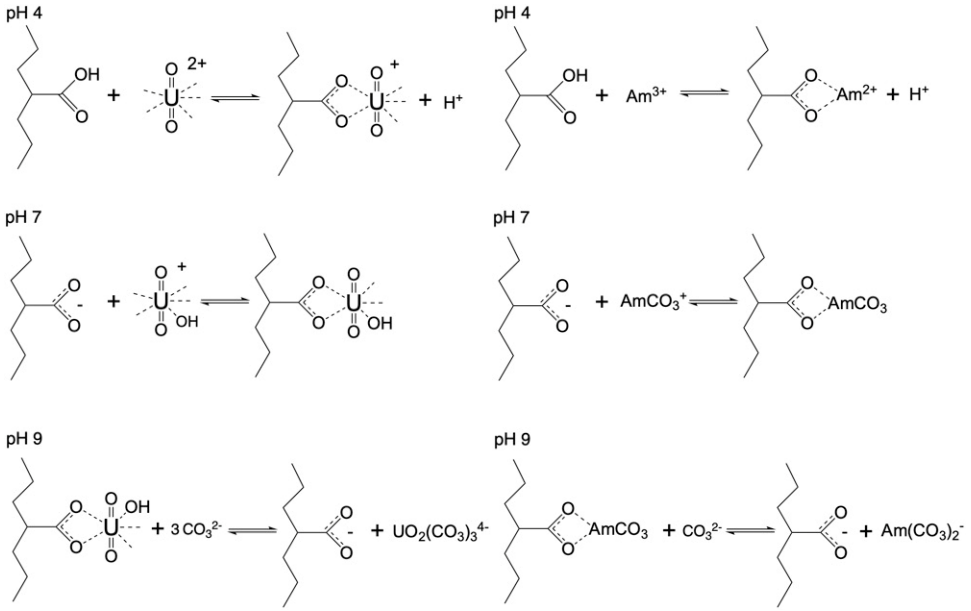

Figure 4. Schematic illustration of probable U(VI) and Am(III) binding by the oxidized carbon fabrics under acidic and alkaline pH conditions.

The associated K_d values, which are summarized in **Figure 5**, show that the K_d values of U(VI) are almost one order of magnitude higher than the corresponding values of Am(III), indicating the higher affinity of the oxidized carbon fabrics for uranium. Nevertheless, the K_d values are lower than the K_d values determined for the adsorption of U(VI) and Am(III) by aerogel [43] and oxidized biochar fibbers [44] and higher than the K_d values determined for the adsorption of the respective radionuclides by microplastics [6,45,46]. These K_d values assume that the oxidized carbon fabrics are excellent adsorbents for the removal of radionuclides from waters even at ultra-trace concentrations and thus could be used in water treatment technologies for the efficient removal of radionuclides from radioactively contaminated waters.

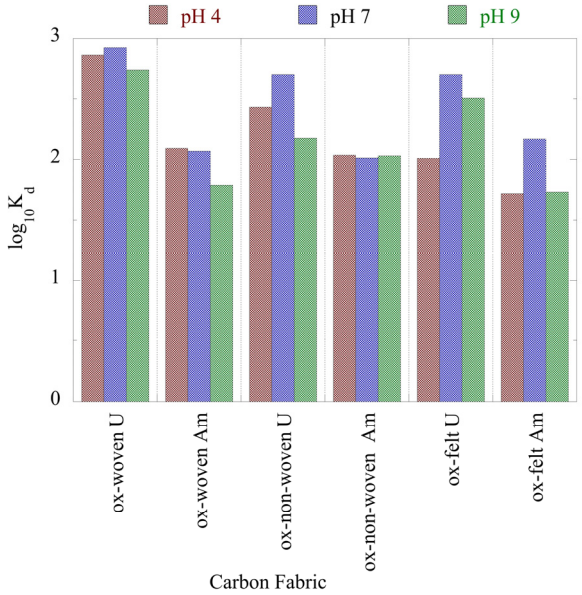

Figure 5. Adsorption efficiency (K_d values) associated with the adsorption of radionuclides (U-232 and Am-241) by three oxidized carbon fabrics from aqueous solution in the acidic (pH 4), neutral (pH

Preprints (www.preprints.org) | NOT PEER-REVIEWED | Posted: 13 November 2023 doi:10.20944/preprints202311.0743.v1

7) and alkaline (pH 9) region. Experimental conditions: 0.5 Bq/mL tracers of U-232 and Am-241 in 10 mL total volume and ambient conditions.

3.2.1. Adsorption Kinetics

The adsorption of radionuclides by the carbon fabrics is a relatively slow process and takes about 10 days until a state of equilibrium is reached (**Figure 6**). This is common for adsorption studies performed at ultra-trace radionuclide concentration because the adsorption kinetics is limited by the radionuclide diffusion from the solution to the adsorbent's surface [23]. Generally, U(VI) is adsorbed faster than Am(III), most probably due to the higher affinity of the surface active moieties (e.g., carboxylic groups) for hexavalent uranium.

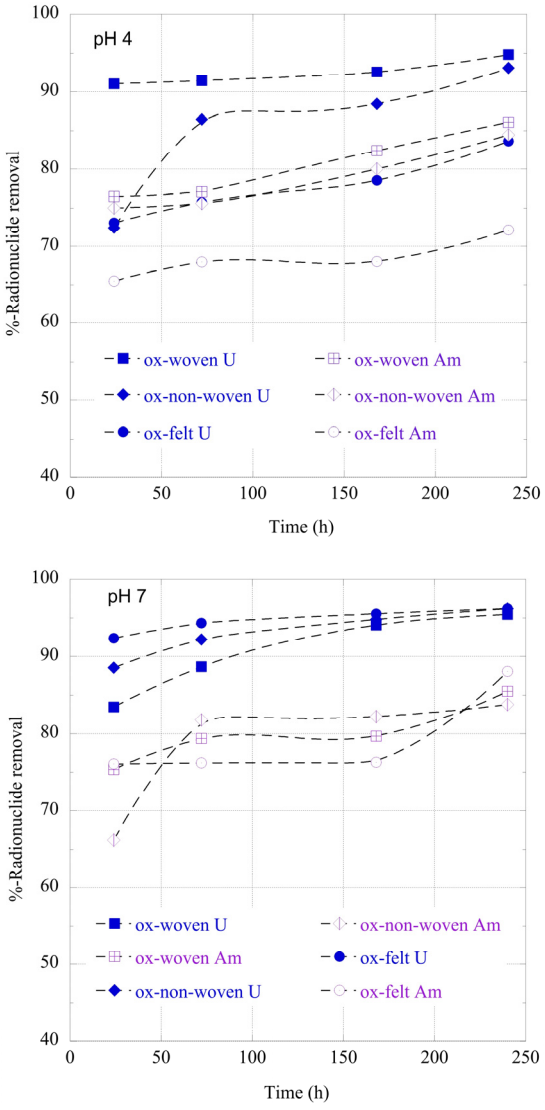

Preprints (www.preprints.org) | NOT PEER-REVIEWED | Posted: 13 November 2023 doi:10.20944/preprints202311.0743.v1

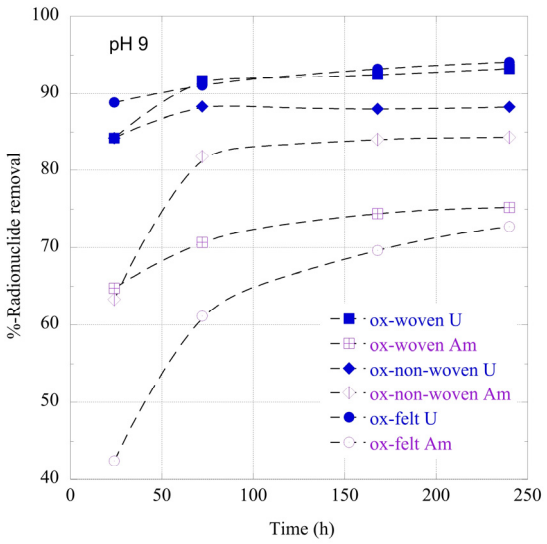

Figure 6. Relative removal of radionuclides (U-232 and Am-241) by the three oxidized carbon fabrics from aqueous solution in the acidic (pH 4), neutral (pH 7) and alkaline (pH 9) region as a function of time. Experimental conditions: 0.5 Bq/mL tracers of U-232 and Am-241 in 10 mL total volume and ambient conditions.

3.2.2. Adsorption Thermodynamics

The effect of temperature on the relative adsorption and associated adsorption thermodynamic parameters (ΔG^o, ΔH^o, ΔS^o) have been evaluated using the experimental adsorption data obtained at three different temperatures. The %-relative adsorption as well as the $\ln K_{ads}$-1/T plots are graphically presented in **Figures 7** and **8**, respectively. For all cases, increasing temperature results in increasing relative adsorption, thus indicating that the radionuclide adsorption by the oxidized carbon fabrics is an endothermic, entropy-driven process. The values of thermodynamic parameters (ΔH^o and ΔS^o) are summarized in **Table 3** and graphically presented in **Figure 9**. This thermochemical behaviour is generally observed for the adsorption of metal ions and other hard metal ions by surface modified carbon-based materials and is associated with the formation of inner-sphere complexes between the surface carboxylate moieties and the radionuclide cations. The adsorption is an entropy-driven process, because upon adsorption and inner-sphere complex formation several water molecules are released from the hydration sphere of the radionuclide ion and hydrated surface carboxylates.

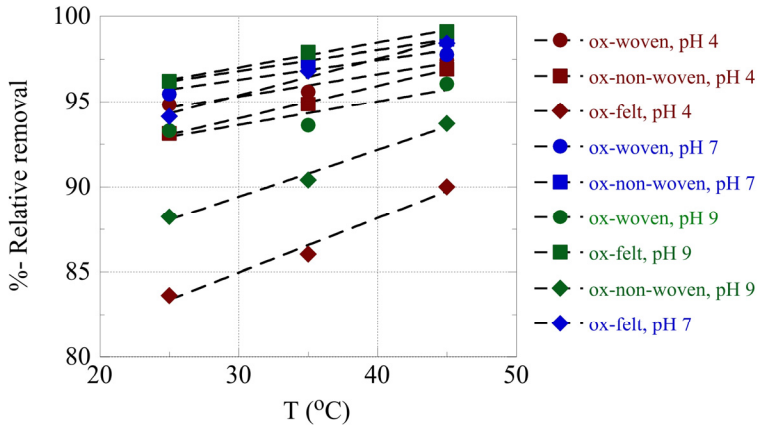

a)

Preprints (www.preprints.org) | NOT PEER-REVIEWED | Posted: 13 November 2023 doi:10.20944/preprints202311.0743.v1

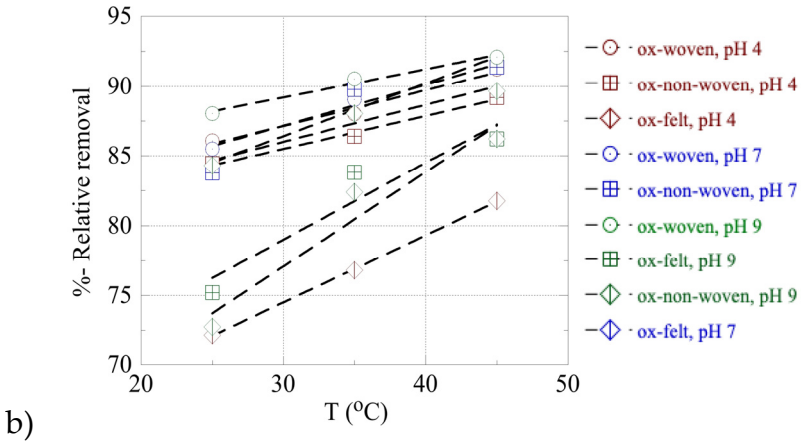

b)

Figure 7. %-relative removal as a function of T for the adsorption of (a) U(VI) and (b) Am(III) by the oxidized carbon fabrics. Experimental conditions: 0.5 Bq/mL tracers of U-232 and Am-241 in 10 mL total volume; the experiments performed under varying pH (4, 7, 9) and temperature (25, 35, 45 °C).

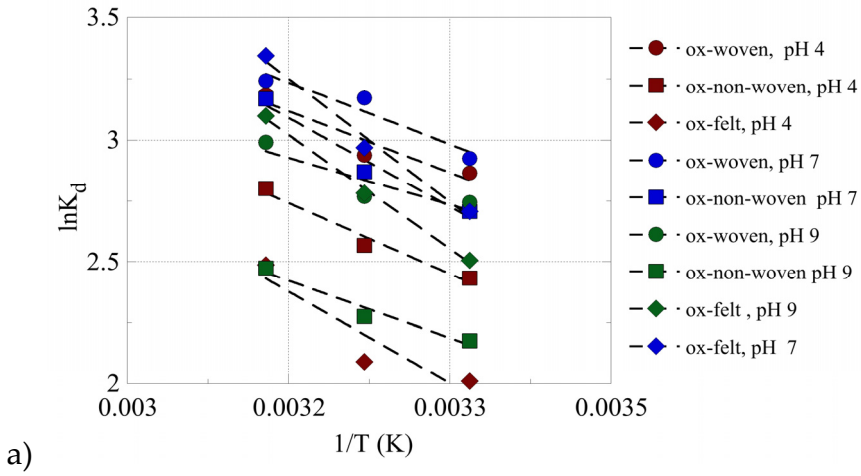

a)

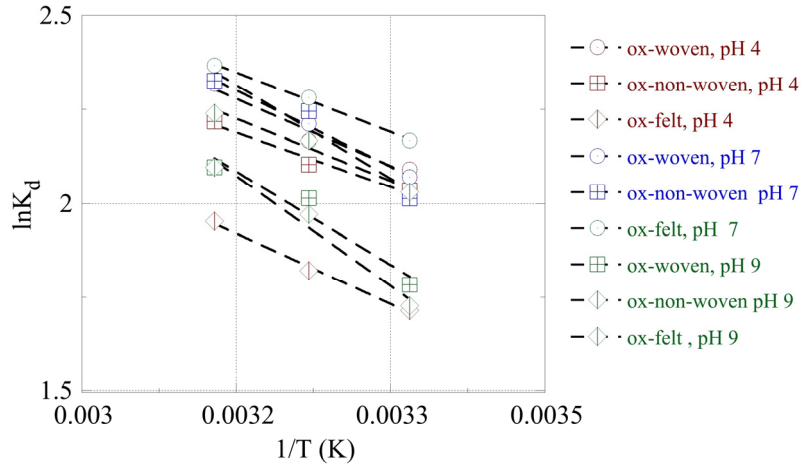

b)

Figure 8. logK$_{ads}$ as a function of 1/T for the adsorption of (a) U(VI) and (b) Am(III) by the oxidized carbon fabrics. Experimental conditions: 0.5 Bq/mL tracers of U-232 and Am-241 in 10 mL total volume; the experiments performed under varying pH (4, 7, 9) and temperature (25, 35, 45 °C).

Preprints (www.preprints.org) | NOT PEER-REVIEWED | Posted: 13 November 2023 doi:10.20944/preprints202311.0743.v1

Table 3. Thermodynamic parameters obtained from the evaluation of the adsorption data at different temperatures.

Material / pH	U(VI)		Am(III)	
	ΔH° (kJ/moL)	ΔS° (J/K·moL)	ΔH° (kJ/moL)	ΔS° (J/K·moL)
Ox-woven / 4	29	151	21	108
Ox-non-woven / 4	34	159	17	94
Ox-felt / 4	43	182	22	106
Ox-woven / 7	29	154	23	118
Ox-non-woven / 7	42	192	29	135
Ox-felt / 7	58	246	18	103
Ox-woven / 9	22	126	29	131
Ox-non-woven / 9	27	132	19	103
Ox-felt / 9	54	228	34	147

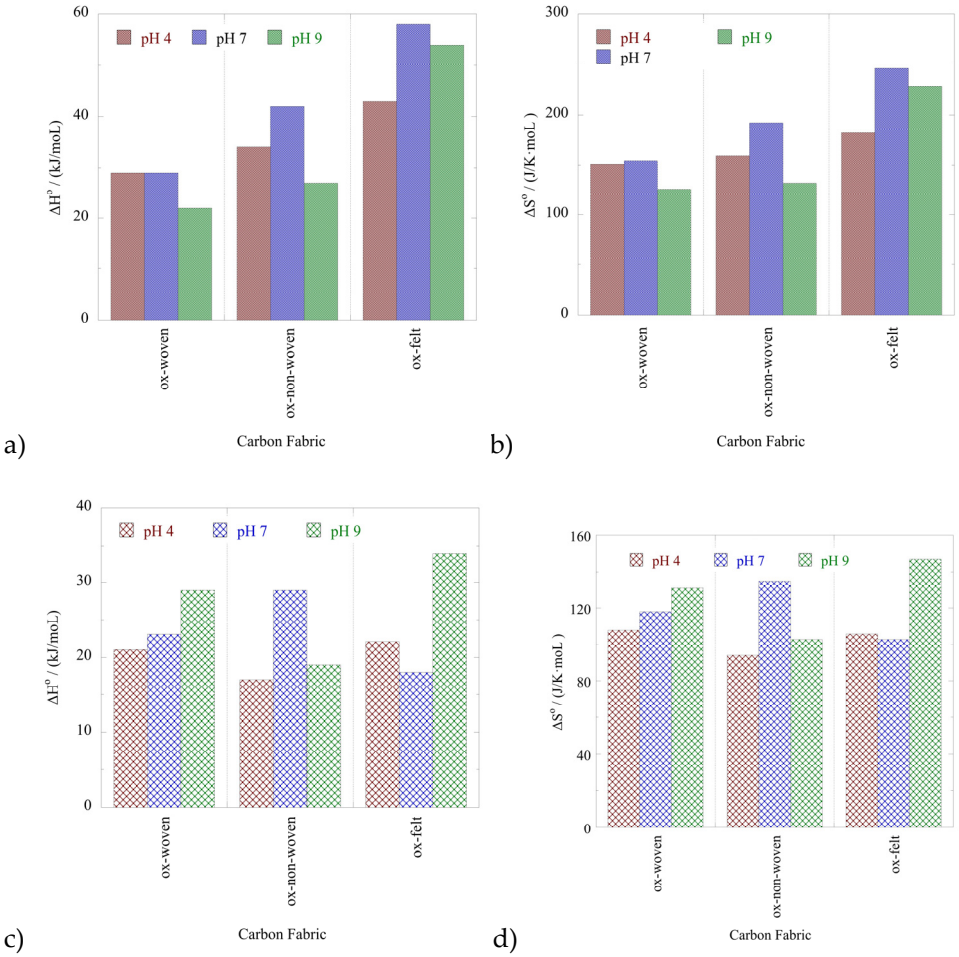

Figure 9. Standard enthalpy (ΔH°) (a, c) and standard entropy (ΔS°) (b, d) values for the adsorption of U(VI) and Am(III) by the oxidized carbon fabrics in de-ionized water solutions at varying pH (4, 7, 9).

Preprints (www.preprints.org) | NOT PEER-REVIEWED | Posted: 13 November 2023 doi:10.20944/preprints202311.0743.v1

3.2.3. Application to Seawater Samples

The radionuclides (U-232 and Am-241) relative removal efficiency and adsorption efficiency (K_d values) by the three oxidized carbon fabrics and the three non-oxidized carbon fabrics in seawater (SW) samples, are shown in **Figures 10** and **11**, respectively. It is evident from **Figure 9** that the relative removal efficiency and adsorption efficiency (K_d values) for oxidized carbon fabrics are reduced in relation to the corresponding values in DI water solutions, after the restoration of equilibrium. Specifically, the relative removal efficiency determined ranges from approximately 45-90% and the adsorption efficiency ($\log(K_d)$) values approximately from 1.5-2.3, with the corresponding values in DI water, pH 9 ranging from 80-98% and 1.8-2.9, respectively. This can be attributed to the presence of various cations (e.g. Ca^{2+} and Fe^{3+}) and anions (e.g. CO_2^{3-}, SO_2^{4}) in the SW solution that compete with U(VI) and Am(III) ions, found in ultra tracers levels, for adsorption on the surface of carbon fabrics. Moreover, the presence of carbonate anions stabilizes U(VI) and Am(III) in solution, forming carbonates such as $UO_2(CO_3)_3^{4-}$ and $Am(CO_2)_2^{-}$.

This decrease in adsorptive capacity in ambient solutions such as SW is attributed to the adsorption of exceptionally low concentrations of radionuclides by various adsorbent materials such as microplastics [6] and aerogels [34]. The K_d values presented by oxidized carbon fabrics in SW are relatively higher than the corresponding values for U-232 and Am-241 adsorption by microplastics [6,44,45] and lower by aerogels [34].

The percentages for the relative removal and the K_d values for the adsorption of radionuclides decrease even further in the case of the non-oxidized (pristine) woven. This observation suggests the importance of the surface chemistry of the adsorbent material. Contrary to the non-oxidized woven, in the case of the oxidized woven the presence of oxo-groups (**Figure 4**) increases the adsorption capacity, as it allows the development of interactions (e.g. dipole cation) between the oxygens on the surface and the various radionuclides (U (VI) and Am(III)).

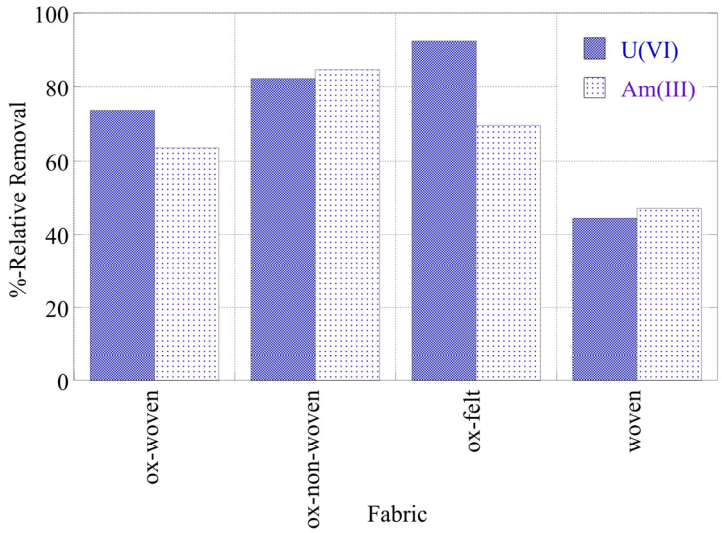

Figure 10. Relative removal of radionuclides (U-232 and Am-241) by three different oxidized carbon fabrics and the woven fabric from seawater solutions (pH 8.3). Experimental conditions: 0.5 Bq/mL tracers of U-232 and Am-241 in 10 mL total volume and ambient conditions.

Preprints (www.preprints.org) | NOT PEER-REVIEWED | Posted: 13 November 2023 doi:10.20944/preprints202311.0743.v1

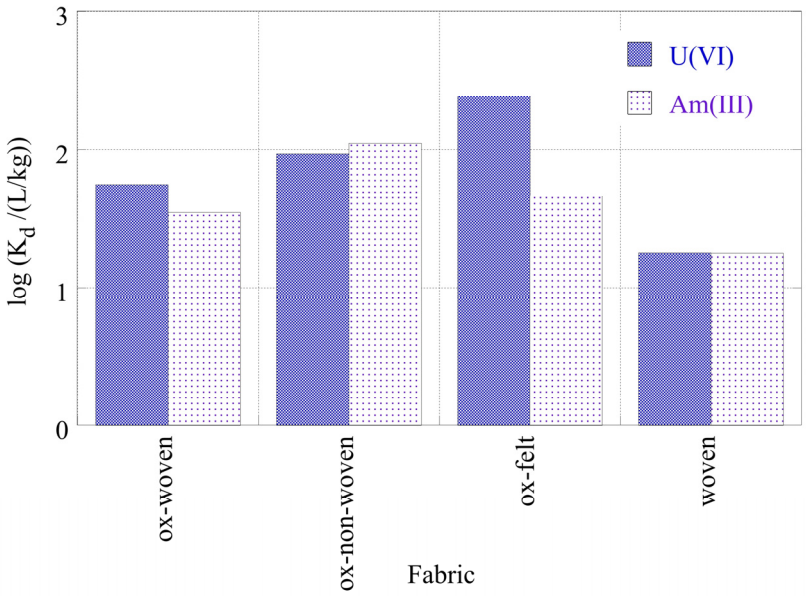

Figure 11. Adsorption efficiency (K_d values) associated with the adsorption of radionuclides (U-232 and Am-241) by three different oxidized carbon fabrics and the woven fabric from seawater solutions (pH 8.3). Experimental conditions: 0.5 Bq/mL tracers of U-232 and Am-241 in 10 mL total volume and ambient conditions.

4. Conclusions

U(VI) and Am(III)adsorption by oxidized carbon fabrics has been investigated in DI water at various pH (4, 7, 9) and SW (pH 8.3). The carbon fabrics present a higher chemical affinity for U(VI) (relative removal efficiency >80%) than Am(III) (relative removal efficiency >70%) at all pHs studied in DI water. In fact, the K_d values of U(VI) are almost an order of magnitude higher than the corresponding values of Am(III). Higher adsorption capacity for U(VI) is observed at neutral pH while decreasing at slightly acidic and alkaline pH. This is due to the partial protonation of the carboxyl groups and the presence of anions (CO_2^{2-}) that stabilize the U(VI) in acidic and alkaline solution, respectively. In the case of Am(III) adsorption by the oxidized non-woven fabric, pH does not seem to significantly affect the adsorption. On the contrary, in the case of oxidized woven and felt fabrics, the adsorption of Am(III) is significantly affected by pH, especially at pH 9. Regarding the experiments carried out in SW, the adsorption capacity for both radionuclides is reduced due to competitive behavior of the various cations (e.g. Ca^{2+} and Fe^{3+}) and anions (e.g. CO_2^{3-}, SO_2^{4-}) present in the solution. Adsorption of the two radionuclides is a relatively slow process, with U(VI) being absorbed faster than Am(III). On the other hand, adsorption is favored by increasing temperature, as in all cases the relative adsorption increases with increasing temperature, indicating that the adsorption of U(VI) and Am(III) is an endothermic and entropy-driven process.

This is of particular importance since carbon fabrics can be easily adapted to existing filtration and water treatment systems and could be a cost-effective substitute for activated carbon powders and granules in adsorption-based water treatment technologies.

Author Contributions: Conceptualization, I.P. and C.R.; methodology, I.I. and I.P.; validation, I.I., I.P. and B.M.; formal analysis, I.I., I.P., B.M. and N.K.; investigation, I.I., B.M., G.K., K.I.., G.C. and N.K.; resources, I.P., N.K and C.R.; data curation, I.I., B.M., G.K. and K.I.; writing—original draft preparation, I.I., I.P., N.K. and C.R.; writing—review and editing, I.I., I.P., G.C., N.K. and C.R..; visualization, I.I., B.M. and N.K.; supervision, I.P. and C.R.; project administration, C.R..; funding acquisition, I.P and C.R. All authors have read and agreed to the published version of the manuscript.

Funding: This research received no external funding, was supported by the University of Cyprus.

Data Availability Statement: The data presented in this study are available on request from the corresponding authors.

Acknowledgments: The authors are grateful to Dr. Mark Baker and Dr. Steve Hinder from the University of Surrey (UK) for providing the XPS-derived elemental compositions of the studied materials. N.K. would like to thank Prof. Christian Mitterer and Prof. Oskar Paris from the Montanuniversität Leoben for providing access to the gas sorption analyzer.

Conflicts of Interest: The authors declare no conflict of interest.

References

1. Inglezakis, V. J.; Poulopoulos, S. G.; Arkhangelsky, E.; Zorpas, A. A.; Menegaki, A. N. Aquatic Environment. In Environment and Development, 137-212, 2016.
2. Lariviere, D.; Taylor, V. F.; Evans, R. D.; Cornett, R. J. Radionuclide Determination in Environmental Samples by Inductively Coupled Plasma Mass Spectrometry. *Spectrochimica Acta Part B: Atomic Spectroscopy* 2006, *61*(8), 877-904.
3. Xu, Mengyu. Syntheses, Structures, and Solution Behavior of Organic-Functionalized Uranyl Peroxide Nanoclusters. University of Notre Dame, 2021.
4. Ewing, R. C. Ceramic Matrices for Plutonium Disposition. *Progress in Nuclear Energy* 2007, *49*(8), 635-643.
5. Humphrey, U. E.; Khandaker, M. U. Viability of Thorium-Based Nuclear Fuel Cycle for the Next Generation Nuclear Reactor: Issues and Prospects. *Renewable and Sustainable Energy Reviews* 2018, *97*, 259-275.
6. Ioannidis, I.; Kinigopoulou, V.; Giannakoudakis, D. A.; Arkas, M.; Anastopoulos, I.; Triantafyllidis, K. S.; Pashalidis, I. Microplastics and Disposable Face Masks as "Trojan Horse" for Radionuclides Pollution in Water Bodies—A Review with Emphasis on the Involved Interactions. *Sustainable Chemistry for the Environment* 2023, 100005.
7. Kouzes, R. T.; Siciliano, E. R.; Ely, J. H.; Keller, P. E.; McConn, R. J. Passive Neutron Detection for Interdiction of Nuclear Material at Borders. *Nuclear Instruments and Methods in Physics Research Section A: Accelerators, Spectrometers, Detectors and Associated Equipment* 2008, *584*, 383-400.
8. Osváth, S.; Vajda, N.; Molnár, Z. Development of a Complex Method for the Determination of Actinides. *J. Radioanal. Nucl. Chem.* 2009, *281*, 461–465.
9. Zhao, B.; Chen, X.; Chen, H.; Zhang, L.; Li, J.; Guo, Y.; Sun, Z. Biomineralization of Uranium by Desulfovibrio desulfuricans A3-21ZLL under Various Hydrochemical Conditions. *Environmental Research* 2023, *237*, 116950.
10. Georgiou, E.; Raptopoulos, G.; Anastopoulos, I.; Giannakoudakis, D. A.; Arkas, M.; Paraskevopoulou, P.; Pashalidis, I. Uranium Removal from Aqueous Solutions by Aerogel-Based Adsorbents—A Critical Review. *Nanomaterials* 2023, *13*(2), 363.
11. Collins, R. N.; Saito, T.; Aoyagi, N.; Payne, T. E.; Kimura, T.; Waite, T. D. Applications of Time-Resolved Laser Fluorescence Spectroscopy to the Environmental Biogeochemistry of Actinides. *J. Environ. Qual.* 2011, *40*, 731-741.
12. Migaszewski, Z. M.; Gałuszka, A. The Use of Rare Earth Element Profiles as a Proxy for Fractionation Source and Mine-Waste Provenance. *Sci. Total Environ.* 2023, *901*, 166517.
13. Debruyne, D.; Hulsbosch, N.; Muchez, P. Unraveling Rare Earth Element Signatures in Hydrothermal Carbonate Minerals Using a Source–Sink System. *Ore Geol. Rev.* 2016, *72*, 232-252.
14. Wang, J.; Shao, L.; Wang, X. The Coal-Forming Environment at the End of the Late Permian and Its Control on Trace Elements: The Upper Xuanwei Formation in Eastern Yunnan, China. *Processes* 2023, *11*(10), 2936.
15. Meinrath, G.; Volke, P.; Helling, C.; Dudel, E. G.; Merkel, B. J. Determination and Interpretation of Environmental Water Samples Contaminated by Uranium Mining Activities. *Fresenius' J. Anal. Chem.* 1999, *364*, 191-202.
16. Wang, Z.; Huang, L.; Dong, X.; Wu, T.; Qing, Q.; Chen, J.; ... & Xu, C. Ion Sieving in Graphene Oxide Membrane Enables Efficient Actinides/Lanthanides Separation. *Nat. Commun.* 2023, *14*, 261.
17. Nash, K. L. Separation Chemistry for Lanthanides and Trivalent Actinides. In Handbook on the Physics and Chemistry of Rare Earths, Vol. 18; 1994; pp. 197-238.
18. Seo, S. D.; Truong-Lam, H. S.; Jeon, C.; Han, J.; Kang, K.; Lee, S.; & Lee, J. D. Simultaneous Removal of Multi-Nuclide (Sr2+, Co^{2+}, Cs^{+}, and I^{-}) from Aquatic Environments Using a Hydrate-Based Water Purification Process. *J. Hazard. Mater.* 2023, 132700.
19. Taylor, P. A. Physical, Chemical, and Biological Treatment of Groundwater at Contaminated Nuclear and NORM Sites. In Environmental Remediation and Restoration of Contaminated Nuclear and NORM Sites; Woodhead Publishing: 2015; pp. 237-256.
20. Khedr, M. G. Radioactive Contamination of Groundwater: Special Aspects and Advantages of Removal by Reverse Osmosis and Nanofiltration. *Desalination* 2013, *321*, 47-54.

21. Gäfvert, T.; Ellmark, C.; Holm, E. Removal of Radionuclides at a Waterworks. *J. Environ. Radioact.* 2002, *63*, 105-115.
22. Kucserka, T.; Németh, G. I.; Pálfi, I.; Kiss, Z. L.; Tombácz, E.; Galambos, I. Adsorption-Based Pretreatment of Irrigation Water to Prevent Water Quality Issues. *Separations* 2023, *10*, 468.
23. Habineza, A.; Zhai, J.; Ntakirutimana, T.; Qiu, F. P.; Li, X.; Wang, Q. Heavy Metal Removal from Wastewaters by Agricultural Waste Low-Cost Adsorbents: Hindrances of Adsorption Technology to the Large Scale Industrial Application—A Review. *Desalin. Water Treat.* 2017, *78*, 192-214.
24. Ibrahim, A. O.; Adegoke, K. A.; Adegoke, R. O.; AbdulWahab, Y. A.; Oyelami, V. B.; Adesina, M. O. Adsorptive Removal of
25. Gusain, R.; Kumar, N.; Ray, S. S. Recent Advances in Carbon Nanomaterial-Based Adsorbents for Water Purification. *Coord. Chem. Rev.* 2020, *405*, 213111.
26. Kostoglou, N.; Koczwara, C.; Prehal, C.; Terziyska, V.; Babic, B.; Matovic, B.; Constantinides, G.; Tampaxis, C.; Charalambopoulou, G.; Steriotis, T.; Hinder, S.; Baker, M.; Polychronopoulou, K.; Doumanidis, C.; Paris, O.; Mitterer, C.; Rebholz, C. Nanoporous Activated Carbon Cloth as a Versatile Material for Hydrogen Adsorption, Selective Gas Separation, and Electrochemical Energy Storage. *Nano Energy* 2017, *40*, 49-64.
27. Pendolino, F.; Armata, N. Graphene Oxide in Environmental Remediation Process; Springer: Switzerland, 2017 7, 11.
28. Nunes, S.P.; Culfaz-Emecen, P.Z.; Ramon, G.Z.; Visser, T.; Koops, G.H.; Jin, W.; Ulbricht, M. Thinking the Future of Membranes: Perspectives for Advanced and New Membrane Materials and Manufacturing Processes. J. Membr. Sci. 2020, 598, 117761.
29. Jia, R.; Sun, D.; Dang, Y.; Meier, D.; Holmes, D. E.; Smith, J. A. Carbon Cloth Enhances Treatment of High-Strength Brewery Wastewater in Anaerobic Dynamic Membrane Bioreactors. *Bioresource Technology* 2020, *298*, 122547.
30. Nieto-Delgado, C.; Partida-Gutierrez, D.; Rangel-Mendez, J. R. Preparation of activated carbon cloths from renewable natural fabrics and their performance during the adsorption of model organic and inorganic pollutants in water. *Journal of Cleaner Production* 2019, *213*, 650-658.
31. Guedidi, H.; Reinert, L.; Sonde, Y.; Bellakhal, N.; Duclaux, L. Adsorption of ibuprofen from aqueous solution on chemically surface-modified activated carbon cloths. *Arabian Journal of Chemistry* 2017, *10*, S3584-S3594.
32. Masson, S.; Gineys, M.; Delpeux-Ouldriane, S.; Reinert, L.; Guittonneau, S.; Béguin, F.; Duclaux, L. Single, binary, and mixture adsorption of nine organic contaminants onto a microporous and a microporous/mesoporous activated carbon cloth. *Microporous and Mesoporous Materials* 2016, *234*, 24-34.
33. Kim, C.; Srimuk, P.; Lee, J.; Fleischmann, S.; Aslan, M.; Presser, V. Influence of pore structure and cell voltage of activated carbon cloth as a versatile electrode material for capacitive deionization. *Carbon* 2017, *122*, 329-335.
34. Alkhaldi, T.; Blankenship, L. S.; Mokaya, R. A simple, sustainable route to flexible microporous carbon cloth for energy storage applications. *Materials Advances* 2023, *4*(16), 3559-3571.
35. Li, Y.; Chen, B.; Gao, Y.; Zhang, J.; Wang, B. Optimization performance of viscose rayon derived flexible porous carbon cloths in relation to their CO_2 capture, CO_2/CH_4 separation and methanol adsorption. *Colloids and Surfaces A: Physicochemical and Engineering Aspects* 2023, *677*, 132350.
36. Attia, N. F.; Jung, M.; Park, J.; Jang, H.; Lee, K.; Oh, H. Flexible nanoporous activated carbon cloth for achieving high H2, CH4, and CO_2 storage capacities and selective CO_2/CH_4 separation. *Chemical Engineering Journal* 2020, *379*, 122367.
37. Jung, M.; Park, J.; Cho, S.Y.; Elashery, S.A.E.; Attia, N.F.; Oh, H. Flexible carbon sieve based on nanoporous carbon cloth for efficient CO_2/CH_4 separation. *Surfaces and Interfaces* 2021, 23, 100960.
38. Liatsou, I.; Pashalidis, I.; Oezaslan, M.; Dosche, C. Surface Characterization of Oxidized Biochar Fibers Derived from Luffa Cylindrica and Lanthanide Binding. *J. Environ. Chem. Eng.* 2017, *5*, 4, 4069-4074.
39. Zulfiqar, U.; Kostoglou, N.; Thomas, A.; Rebholz, C.; Matthews, A.; Lewis, D.J. Flexible Nanoporous Activated Carbon for Adsorption of Organics from Industrial Effluents. *Nanoscale* 2021, *13*, 15311-15323.
40. Hadjittofi, L.; Pashalidis, I. Uranium Sorption from Aqueous Solutions by Activated Biochar Fibres Investigated by FTIR Spectroscopy and Batch Experiments. J. *Radioanal. Nucl. Chem.* 2015, *304*, 897-904.
41. Kiliari, T.; Pashalidis, I. Simplified Alpha-Spectroscopic Analysis of Uranium in Natural Waters after Its Separation by Cation-Exchange. *Radiat. Meas.* 2010, *45*, 966-968.
42. Thommes, M.; Kaneko, K.; Neimark, A.V.; Olivier, J.P.; Rodriguez-Reinoso, F.; Rouquerol, J.; Sing, K.S.W. Physisorption of Gases, with Special Reference to the Evaluation of Surface Area and Pore Size Distribution (IUPAC Technical Report). *Pure Appl. Chem.* 2015, *87*, 1051-1069.
43. Ioannidis, I.; Pashalidis, I.; Raptopoulos, G.; Paraskevopoulou, P. Radioactivity/Radionuclide (U-232 and Am-241) Removal from Waters by Polyurea-Crosslinked Alginate Aerogels in the Sub-Picomolar Concentration Range. *Gels* 2023, *9*, 211.

44. Kazakis, N.; Busico, G.; Ntona, M.M.; Philippou, K.; Kaprara, E.; Mitrakas, M.; Voudouris, K. The Origin of Uranium in Groundwater of the Eastern Halkidiki Region, Northern Greece. *Sci. Total Environ.* 2022, *812*, 152445.
45. Ioannidis, I.; Anastopoulos, I.; Pashalidis, I. Microplastics as Radionuclide (U-232) Carriers. *J. Mol. Liq.* 2022, *351*, 118641.
46. Ioannidis, I.; Xenofontos, A.; Anastopoulos, I.; Pashalidis, I. Americium Sorption by Microplastics in Aqueous Solutions. *Coatings* 2022, *12*, 1-9.